

Optimal Experiments with Seismic Sensors for the Localization of Buried Landmines

Mubashir Alam^a, Gregg D. Larson^b, James H. McClellan^a, and Waymond R. Scott Jr^a

^aSchool of Electrical and Computer Engineering

^bSchool of Mechanical Engineering

Georgia Institute of Technology, Atlanta, Georgia 30332-0250

ABSTRACT

In this paper, we consider the problem of detecting and locating buried land mines and subsurface objects by using seismic waves. We demonstrate an adaptive seismic system that maneuvers an array of receivers, according to an optimal positioning algorithm based on the theory of optimal experiments, to minimize the number of distinct measurements to localize the mine. The adaptive localization algorithm is tested using numerical model data as well as laboratory measurements performed in a facility at Georgia Tech. Cases with one and two targets are presented. It is envisioned that future systems should be able to incorporate this new method into portable mobile mine-location systems.

Keywords

Optimal Experiments, Array Imaging, Seismic, Landmine Detection

1. INTRODUCTION

Buried land mines and similar subsurface structures pose a huge threat to resettling civilians. It takes significant time and resources to clear out regions contaminated by mines, so it is important to develop efficient detection and localization systems to create a safer environment. Georgia Tech has built a laboratory to collect the real data needed to investigate buried land mine and subsurface target detection problems [1]. In the laboratory settings, the detection schemes using seismic and acoustic waves have been extensively tested [1–4]. These methods present solutions with satisfactory mine detection probabilities.

The use of seismic waves to detect subsurface targets complements existing systems, which are usually based on Ground Penetrating Radar (GPR) and Electromagnetic Induction (EMI) sensing. Seismic waves, scattered from man-made targets, induce resonances that result in a stronger sustained reflection from mines than from clutter objects. Hence, it is possible to use seismic imaging to discriminate land mines from common types of clutter such as rocks, wood, etc. To detect a mine, a seismic wave is launched from a source at a known location. The seismic wave then travels through the soil and interacts with objects under the ground. The resulting propagating waves in an elastic medium are of two main types: surface waves and body waves. The existing research concentrates on reflected surface waves (Rayleigh waves) for detection, because the Rayleigh waves carry the most of the returned energy.

In general, typical imaging methods are time consuming, and expensive measurements must be taken over 2-D grids with large apertures to have sufficient image resolution over the space of interest. Once a complete image is formed from a large data set, it is searched to find targets [4]. However, to image any single target, only a small subset of the measurements is actually required, but we do not know this subset ahead of time. Therefore, if we want to reduce the time or resources needed to localize a target, we can use maneuvering receiver(s) to take the minimum number of measurements needed, if we can develop an adaptive algorithm to find the best receiver positions. With each new measurement, we want to maximize the information gained about the target. In our case, we use a maneuvering 3×3 array to create an efficient system to detect and locate mines. In the method proposed here, any one image, created at successive measurements, has low resolution. However, as the array maneuvers, the cumulative imaging operation improves the resolution around the true mine location. Hence, even with a small array we can overcome the problem of low resolution, by increasing the effective aperture with cumulative imaging.

The array movement is based on the theory of optimal experiments [5]. Starting with a 2-D sensor array with known relative positions, an initial estimate of the target location is made. Then, the variance of the location estimate is calculated from the Fisher information matrix (FIM). Based on the expected value of the FIM, the next optimal array position is determined by using the theory of optimal experiments [5,6]. The search for the optimal array position maximizes the determinant of the Fisher information matrix. The two steps involved in the maneuver strategy for a mobile array of sensors are shown in Figs. 1(a) and 1(b).

The organization of the paper is as follows. Section 2 formulates the problem and the data model for seismic signals. Section 3 describes the algorithm for estimating the target position along with performance bounds. Section 4 describes how the theory of optimal experiments is used to find the next array position. Sections 5, 6 and 7 describe the results of applying the algorithm to experimental data collected in a laboratory setting [2].

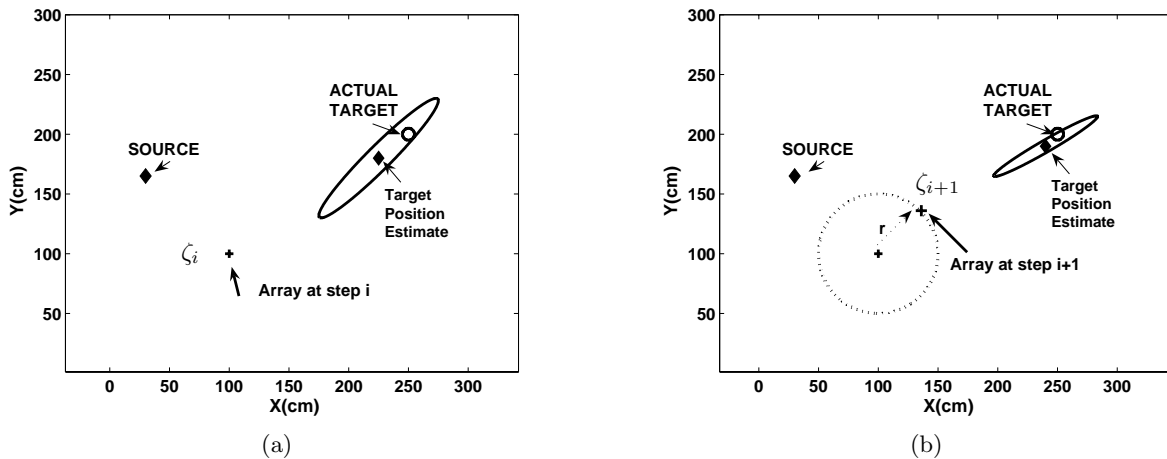


Figure 1. Algorithm mechanics illustrated: (a) Source generates a probing pulse. The waves are reflected from a target and are collected by means of an array. At step i , the target position z_i is estimated when the array center is at ζ_i (b) Estimate the next array position ζ_{i+1} by using the estimated target position z_i and the constrained cumulative Fisher Information Matrix measure.

2. DATA MODEL FOR ACTIVE SENSING

Consider a single seismic source and an array of P seismic receivers, where the source and receivers lie in the same surface plane. Assume that there are K targets. We model the soil as a highly dispersive medium with frequency dependent velocity. Hence, the signal processing is done in the frequency domain, even though the measurements are taken in the time domain.

The received seismic data at frequency ω can be written as

$$\mathbf{y}(\omega) = \mathbf{G}(\omega)\mathbf{D}(\omega)\mathbf{g}_1(\omega) + \mathbf{n}(\omega), \quad (1)$$

where $\mathbf{g}_1(\omega)$ is a $K \times 1$ vector that models the propagation from the single seismic source to the targets, $\mathbf{D}(\omega)$ is a $K \times K$ diagonal matrix whose diagonal elements represents scattering coefficients, $\mathbf{G}(\omega)$ is a $P \times K$ matrix that represents the propagation from targets back to the receiver array, and $\mathbf{n}(\omega)$ the additive noise vector [7–10]. The elements of the propagation matrices are given by the 2-D Green's function. Since only the signal reflected from the target is of interest, the active system in (1) can be simplified to the following passive system

$$\mathbf{y}(\omega) = \mathbf{G}(\omega)\mathbf{s}(\omega) + \mathbf{n}(\omega), \quad (2)$$

where $\mathbf{D}(\omega)\mathbf{g}_1(\omega)$ has been replaced by a $K \times 1$ signal vector $\mathbf{s}(\omega)$ that represents the reflected signal from targets. Equation (2) has the same mathematical form as the narrow-band data model [11] used in conventional array signal processing and this similarity will be exploited while calculating the likelihood statistics.

In the seismic problem, the elements of the propagation matrix $\mathbf{G}(\omega)$ are given by the illuminating Green's vector (steering vector) [7–9, 12],

$$\mathbf{g}(\mathbf{z}, \mathbf{x}, \omega) = [\tilde{g}(\mathbf{z}, \mathbf{x}_1, \omega), \tilde{g}(\mathbf{z}, \mathbf{x}_2, \omega), \dots, \tilde{g}(\mathbf{z}, \mathbf{x}_P, \omega)]^T, \quad (3)$$

where \mathbf{z} is the target position, \mathbf{x}_i represents the i^{th} sensor position in the 2D plane, and the function \tilde{g} is the 2D Green's function, whose analytical form is

$$\tilde{g}(r, r', \omega) = \frac{i}{4} H_0^{(1)} \left(\frac{\omega}{v(\omega)} |r - r'| \right), \quad (4)$$

where $H_0^{(1)}$ is the zero-order Hankel function of the first kind, and $v(\omega)$ is the frequency-dependent Rayleigh wave velocity.

Spectrum analysis of the surface waves can be used to determine the velocity vs. frequency [13]. To minimize confusion when we refer to the existing array processing literature results, we change the notation for the propagation matrix \mathbf{G} to \mathbf{A} (known as the steering matrix in array signal processing problems). The final form of the data model becomes [11]:

$$\mathbf{y}(\omega) = \mathbf{A}(\zeta, \mathbf{z}, \omega) \mathbf{s}(\omega) + \mathbf{n}(\omega), \quad (5)$$

where $\mathbf{y}(\omega) \in \mathcal{C}^{P \times 1}$ is the noisy array output vector, $\mathbf{n}(\omega) \in \mathcal{C}^{P \times 1}$ is a complex additive noise, and $\mathbf{s}(\omega) \in \mathcal{C}^{K \times 1}$ is the signal vector. The array manifold $\mathbf{A}(\zeta, \mathbf{z}, \omega)$ has elements given by the Green's function (3), which depends on the array center position ζ and the (unknown) target position \mathbf{z} . Note that the individual receiver positions \mathbf{x}_i can be related to ζ via the known array geometry. Consequently, our objective is to determine the target position \mathbf{z} given the received array data $\mathbf{y}(\omega)$.

3. TARGET LOCATION ESTIMATION

3.1. Position Parameters Estimate

Let $\mathbf{Y}_t = [\mathbf{y}_t^T(\omega_1), \dots, \mathbf{y}_t^T(\omega_N)]^T$, $\mathbf{Y}_t \in \mathcal{C}^{PN \times 1}$, be the data vector, formed by aggregating the Fourier transform at frequencies ω_i of the received data \mathbf{y}_t at each seismic sensor during the batch period t . Under the *i.i.d.* Gaussian noise assumption, the probability density function for the current received data is given by [14–16]:

$$p(\mathbf{Y}_t) = \prod_{l=1}^N \frac{1}{\pi^P \sigma_t^{2P}} \exp \left\{ -\frac{1}{\sigma_t^2} \|\mathbf{y}_t(\omega_l) - \mathbf{A}_t(\omega_l) \mathbf{s}_t(\omega_l)\|^2 \right\} \quad (6)$$

Using (6), one can calculate the negative log-likelihood function of the data:

$$L^- = NP \log(\pi \sigma_t^2) + \frac{1}{\sigma_t^2} \sum_{l=1}^N \|\mathbf{y}_t(\omega_l) - \mathbf{A}_t(\omega_l) \mathbf{s}_t(\omega_l)\|^2. \quad (7)$$

The Maximum-Likelihood (ML) estimate, maximizing the log-likelihood, can be determined by minimizing L^- . In (7), both the target signal and the noise variance are unknown. Therefore, we first estimate the noise variance by fixing the target position in $\mathbf{A}_t(\omega)$ and the source signal $\mathbf{s}(\omega)$. The ML estimate of the noise variance σ_t^2 is given by:

$$\hat{\sigma}_t^2 = \frac{1}{NP} \sum_{l=1}^N \|\mathbf{y}_t(\omega_l) - \mathbf{A}_t(\omega_l) \mathbf{s}_t(\omega_l)\|^2. \quad (8)$$

When the estimated noise variance is used in conjunction with (7), the ML target signal estimate can be calculated:

$$\hat{\mathbf{s}}_t(\omega_l) = (\mathbf{A}_t^H(\omega_l) \mathbf{A}_t(\omega_l))^{-1} \mathbf{A}_t^H(\omega_l) \mathbf{y}_t(\omega_l). \quad (9)$$

Substituting (8) and (9) in (7), one can determine the ML cost function to minimize as a function of \mathbf{z}

$$J_t(\mathbf{z}) = \sum_{l=1}^N \left\| \left\{ I - \mathbf{A}_t(\omega_l) (\mathbf{A}_t^H(\omega_l) \mathbf{A}_t(\omega_l))^{-1} \mathbf{A}_t^H(\omega_l) \right\} \mathbf{y}_t(\omega_l) \right\|^2 \quad (10)$$

$$= \sum_{l=1}^N \text{trace} \{ P_{A_t}^\perp(\omega_l) R_y(\omega_l) \}, \quad (11)$$

where $P_{A_t}^\perp(\omega_l) = I - \mathbf{A}_t(\omega_l) (\mathbf{A}_t^H(\omega_l) \mathbf{A}_t(\omega_l))^{-1} \mathbf{A}_t^H(\omega_l)$, is the projection onto the null space of $\mathbf{A}_t^H(\omega_l)$ and $R_y(\omega_l) = \mathbf{y}_t(\omega_l) \mathbf{y}_t^H(\omega_l)$ is the single snapshot covariance matrix estimate at the frequency ω_l . The target location estimate is then given by the minimum of the cost function (10)

$$\mathbf{z} = \arg \min_{\mathbf{z}} J_t(\mathbf{z}), \quad (12)$$

where the array location is assumed known.

3.2. Cramér-Rao Lower Bound for the Estimate of \mathbf{z}

The Cramér-Rao lower bound (CRLB) is an information theoretic inequality, which provides a lower bound for the variances of unbiased estimators. If an estimator achieves the CRLB, then it is also a solution of the likelihood equation. The Cramér-Rao lower bound is the inverse of the Fisher information matrix (FIM). Assuming that the variance of the additive noise in (1) is known, the log-likelihood function for a single target can be written as:

$$L(\zeta_t, \mathbf{z}) \doteq -\frac{1}{\sigma_t^2} \sum_{l=1}^N \|\mathbf{y}_t(\omega_l) - \mathbf{a}_t(\zeta_t, \mathbf{z}, \omega_l) s_t(\omega_l)\|^2, \quad (13)$$

where $\mathbf{a}_t(\zeta_t, \mathbf{z}, \omega)$ is the propagation (steering) vector from the array center to the target position. The $(i, j)^{\text{th}}$ element of the FIM is given by the partial derivative of (13) with respect to the i^{th} and j^{th} parameters of the vector \mathbf{z} [14]:

$$\mathbf{F}_{i,j}(\mathbf{z}, \zeta_t) = E_y \left\{ \frac{\partial^2 L(\mathbf{z}, \zeta_t)}{\partial z_i \partial z_j} \right\} \quad (14)$$

$$= -\frac{2}{\sigma_t^2} \sum_{l=1}^N \Re \left\{ \left(\frac{\partial \mathbf{a}_t(\mathbf{z}, \zeta_t, \omega_l)}{\partial z_i} \right)^H \frac{\partial \mathbf{a}_t(\mathbf{z}, \zeta_t, \omega_l)}{\partial z_j} \right\}, \quad (15)$$

where $E_y\{\cdot\}$ denotes the expected value, and \mathbf{F} is the Fisher information matrix (FIM) as a function of the target position \mathbf{z} and the array center ζ . The elements of steering vector are given in terms of 2-D Green's function in (4). The partial derivative of the steering vector is calculated with respect to the target coordinates for a fixed array center.

4. MOVEMENT OF THE SEISMIC ARRAY VIA OPTIMAL EXPERIMENTS

In the previous sections, we described how to determine the target position and its FIM that represents the uncertainty about the estimates as a function of the array center position. Note that the sensors in the 2D array have known locations with respect to the array center ζ . Suppose that we have estimated the target location at batch t , and now we are interested in determining the next optimal array center position candidate for the batch $t+1$. Our approach in selecting the new sensor position reduces the expected uncertainty in the estimated target coordinates by minimizing the determinant of the CRLB. Hence, to minimize the CRLB determinant, we must maximize the determinant of the FIM as a function of the array center. In the optimal experiment literature this technique is called D-optimal design [5]. A similar approach is used in [6] for magnetic sensors. Other approaches might minimize the trace of the CRLB or minimize the maximum eigenvalue of the CRLB.

Let q represent the determinant of the FIM. The cumulative effect of the measurements up to batch t can be written as:

$$q(\{\zeta_1, \dots, \zeta_t\}) = |F(\zeta_1, \dots, \zeta_t)| = \left| \sum_{j=1}^t F(\zeta_j) \right|, \quad (16)$$

where $|\cdot|$ stands for determinant and F_t represents the Fisher information matrix at batch t . The logarithmic increase due to the additional measurements at batch $t + 1$ is given by

$$\begin{aligned} \delta_q(\zeta_{t+1}) &= \ln q(\{\zeta_1, \dots, \zeta_{t+1}\}) - \ln q(\{\zeta_1, \dots, \zeta_t\}) \\ &= \ln |I + F(\zeta_{t+1})B_t^{-1}|, \end{aligned} \quad (17)$$

where I is an identity matrix, and $B_t = \sum_{j=1}^t F(\zeta_j)$. To achieve the maximum expected information gain, the next optimal array center can be determined by

$$\zeta_{t+1} = \arg \max_{\zeta} \ln |I + F(\zeta_{t+1})B_t^{-1}|. \quad (18)$$

In this optimization problem, there are implicit constraints that come from the configuration of the seismic system. First of all, the target reflections do not behave as an omni-directional active source. Hence, we need to make sure that the receiving array is between the source and the targets all the time to receive the reflected waves. One way to impose this condition is to use a movement step size of radius r from the previous array center position. Hence, the maximum of (18) is calculated on a circle of radius r , where the center of the circle is at the previous optimum array center position.

Another way to impose a constraint on the movement would be to add a penalty term as in [6]:

$$\Psi(\zeta) = \delta_q(\zeta_{t+1}) - \nu \sqrt{(\zeta_{t+1} - \zeta_t)^T \Sigma^{-1} (\zeta_{t+1} - \zeta_t)}, \quad (19)$$

where $\nu \geq 0$ is the penalty factor that must be chosen relative to the size of $\delta_q(\zeta_{t+1})$, and Σ is a diagonal matrix, whose diagonal elements are chosen to ensure the smooth movement of the array from its previous position. Because the array might choose a different step size at each batch, depending on the choice of ν , this approach is not preferred by the authors.

5. PROCESSING OF EXPERIMENTAL DATA

An experiment has been conducted in a laboratory setting, where buried mines in a sandbox are used as targets [1]. A shaker is used as a seismic source, and the input signal is a differentiated Gaussian pulse centered at 450Hz. The pulse in the time and frequency domains is shown in Figs. 2(a) and (b), respectively. In the experiment, ground-contacting accelerometers are used as the seismic sensors. The target is a TS-50 (anti-personnel) landmine buried at a depth of 1 cm. We estimate the wave-number for the reflected signals at different frequencies by using the algorithm presented in [13]. To separate the waves, a linear array of fifteen sensors is used, but only three of them are used in the subsequent imaging step.

Typical spectrum plots for the surface wave analysis for buried targets are shown in Figs. 3(a) and (b). The forward and reflected waves appear at different velocities, from which they can be separated and reconstructed in time domain. Once the data is collected and the waves are separated the next step is to estimate the target position. The initial estimate is shown as a surface plot in Fig. 4. The surface plot is obtained by using (10) and this cost function is calculated at each point in the 2D grid. The minimum of this function is the target position estimate. However, the inverse of this function is plotted in Fig. 4. Based on the initial estimate, the next optimal array position is determined by using (18). This function is calculated at each grid point as a function of array center position using the estimated target position from the previous step. The surface plots for both the circle and the measurement constraints are shown in Figs. 5(a) and (b). For the circle constraint, radius of 25 cm is used. For the measurement constraint (19), a relative weighting $\nu = 1.1$ is used, and for the movement penalty matrix Σ , a diagonal matrix with diagonal values of 20^2 is used.

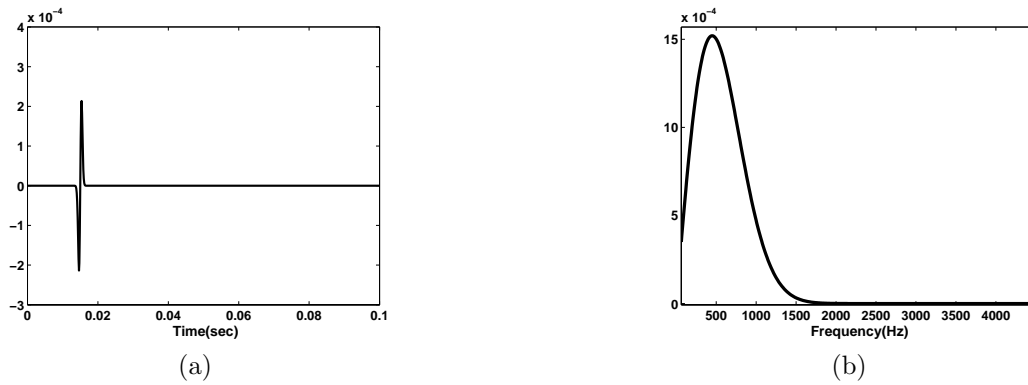


Figure 2. Probing signal is a differentiated Gaussian pulse. (a) Signal amplitude vs. time. (b) Magnitude of the frequency response vs. frequency.

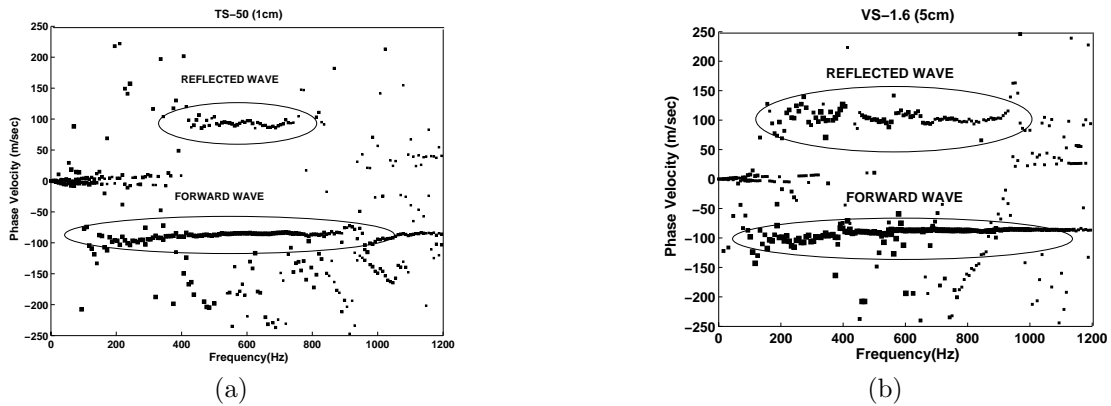


Figure 3. Spectrum analysis of the waves in the presence of buried targets. (a) TS-50 landmine at 1 cm depth. (b) VS1.6 landmine at a depth of 5 cm.

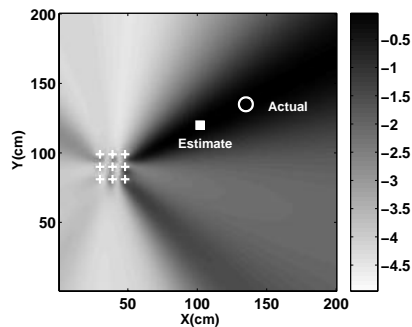


Figure 4. Initial target location estimate is done using the ML cost function (10) (dB scale, inverse of the cost function is plotted).

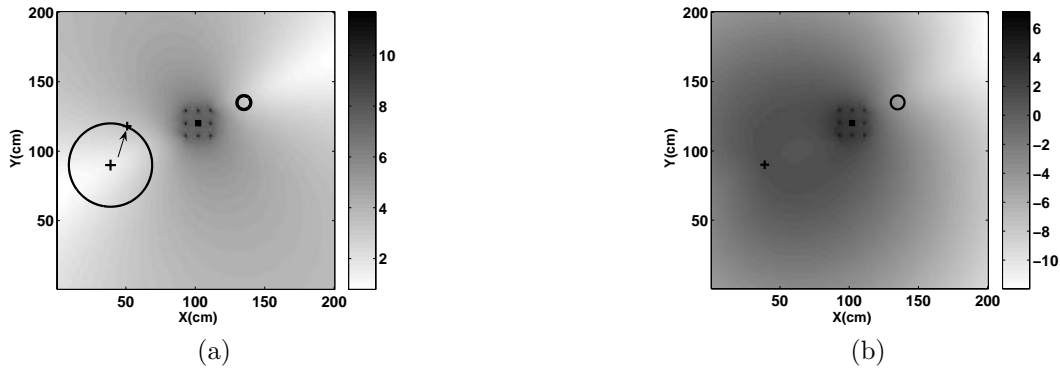


Figure 5. The optimum movement for the next array position can be constrained by (a) a maximum distance within a circle; or by (b) a penalty function. The plotted surface is the determinant of the FIM on a linear scale and, (b) is the FIM determinant plus the penalty term.

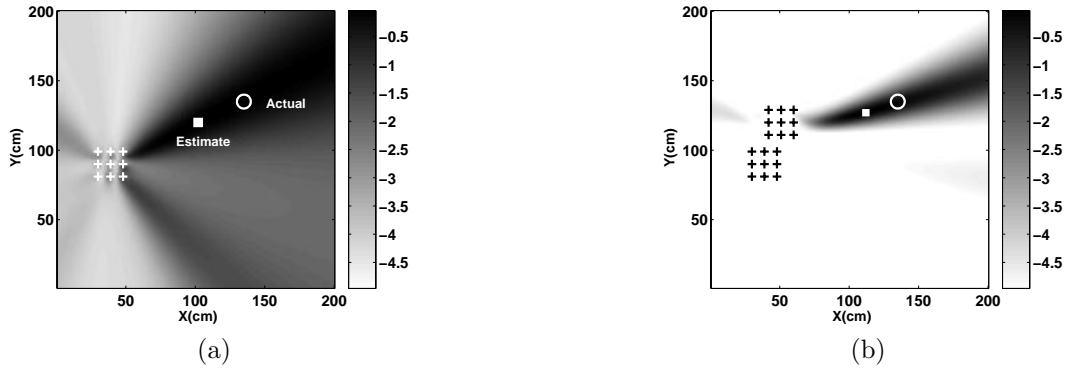


Figure 6. Target position estimates (dB scale, inverse of the cost function is plotted) (a) Initial estimate. (b) Estimate after the optimal move as determined by the circle constraint.

Once the next optimum array position is determined and the array is moved to a new position, a new batch of data is collected. We then append the existing data to the new set of data. The new target position estimate and the next optimum movement are determined by using the cumulative data. Further steps are shown in Figs. 6 and 7. With each successive step the target position estimate is improved, along with a decrease in the uncertainty ellipse because the cumulative estimation is effectively increasing the aperture.

6. REAL-TIME IMPLEMENTATION

The source and receiver setup for the real time experiment is shown in Fig. 8. In this case an anti-tank (AT) mine, VS1.6, is buried at a depth of 5 cm. The AT mine is large with a diameter of roughly 20 cm. The fixed seismic source and the mobile sensor array consisting of 30 elements are also shown. The movement of the array and the firing of the source is controlled by a Labview interface. The probing pulse is the same differentiated Gaussian pulse at a center frequency of 450Hz. The rectangular seismic array consists of three lines each containing ten uniformly spaced sensors.

The data collected across each line of the seismic array is processed by the Prony-based velocity spectrum analysis, and the forward and reverse waves are separated using the spectrum analysis. Three out of the ten sensors in each line are retained to form a 2-D array for imaging. Hence, there are a total of nine sensors arranged in a 3×3 2-D grid. There are two steps involved in the target detection. First we perform a probe phase, where two fixed array positions very near to the source are used to collect the data and form an initial target position estimate by using imaging algorithm. The next phase is the search mode, where the array position is calculated optimally and the target position estimate is refined. Using the optimal maneuver strategy, the

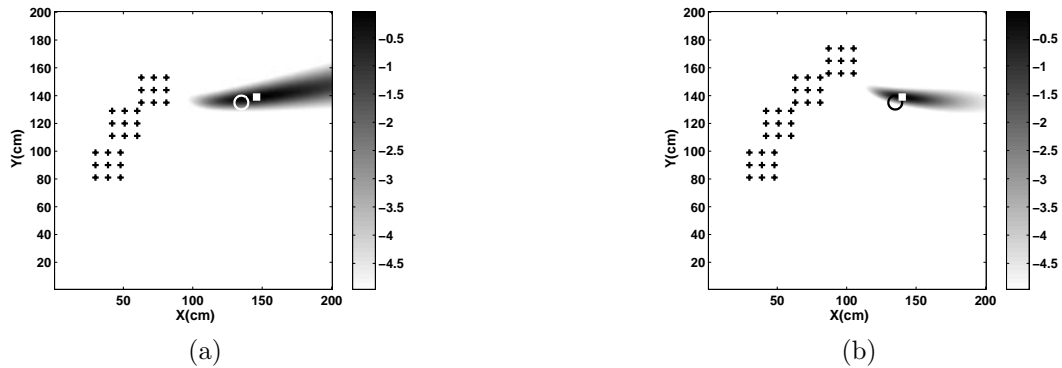


Figure 7. Target position estimate (dB scale, inverse of the cost function is plotted) (a) After two optimal moves. (b) After three optimal moves.

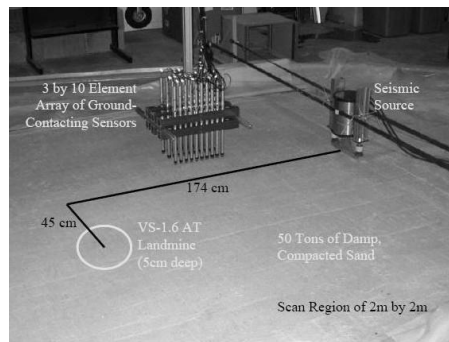


Figure 8. Experimental Setup showing the sensor array of 3 by 10 elements, and the fixed seismic source, and the buried target.

target is found within 3 or 4 iterations, so there is considerable reduction in the number of measurements and total data collection time. In the experiment, the optimal array movement is constrained by the circle constraint, using a radius of 25 cm to control the step size. The first two iterations are the probe phase, and the next three array positions are chosen optimally. All the location estimate results are shown together in Figs. 9 and 10, with the final estimate in Fig. 11. We observe the same behavior as before with the array moving toward the target while increasing the effective aperture, and thereby reducing the size of the uncertainty ellipse around target position estimate. Each iteration took approximately 40 seconds, including all the data acquisition and processing. So in less than 3 or 4 minutes we are able to find the exact position of the target. This should be compared to the existing method, which finds a target in an area of (2×2) m using measurements on a grid of size (100×100) [1, 2, 4]. The complete scan takes several hours to isolate a resonating target.

7. MULTI-TARGET CASE

To simulate a multi-target scenario, two VS1.6 AT mines are buried at the same depth of 5 cm. The goal is to localize both of them with optimal maneuvering. During the probe stage, three fixed array positions with respect to the source are used to find the starting locations for the targets. These array positions are shown in Fig. 12, but only the array center positions are shown, the shape and size of the array is the same as in the real-time implementation example. After the initial location estimates have been obtained, we can start to maneuver the array optimally with the FIM. Since we have two targets in this case, the Fisher information matrix is of size 4×4 . The matrix can be partitioned into four 2×2 quadrants related to individual targets and their cross terms.

Since we have to use the Fisher information matrix in (18), there are various options available. One is to use the full 4×4 FIM matrix in (18), and the other is to use a partitioned approach with two smaller 2×2 FIMs, one for each target. The second case involves multi-objective optimization to satisfy both measures. Using the

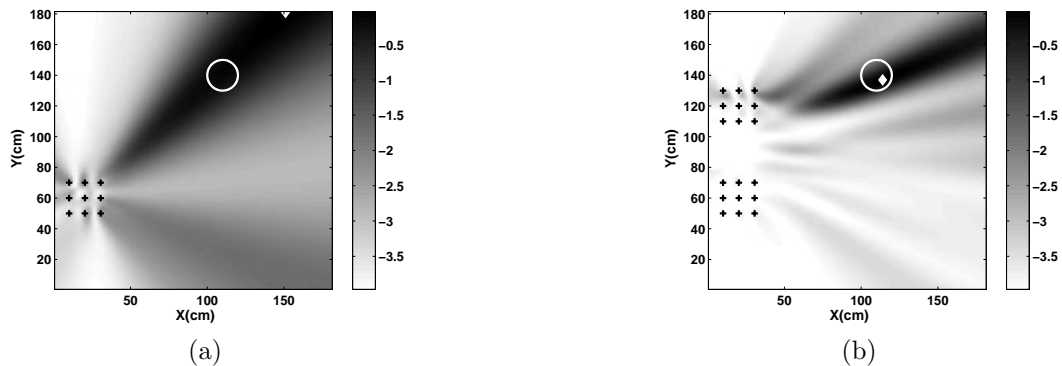


Figure 9. Maximum likelihood surfaces at probing steps (dB scale, inverse of the cost function is plotted) (a) At the initial data collection, the uncertainty around the estimated target position is large. (b) The optimal movement reduces the uncertainty under the constant movement distance constraint.

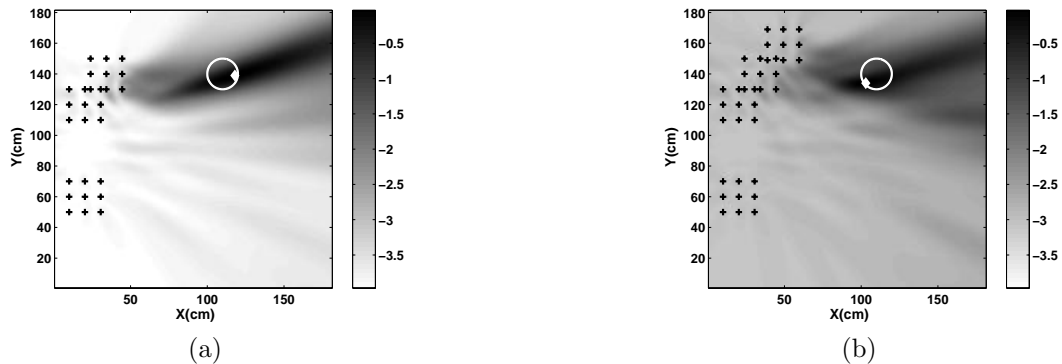


Figure 10. Other optimal maneuvers for the target position estimation are shown (dB scale, inverse of the cost function is plotted) (a) The movement direction tries to reduce the largest eigenvalue of the uncertainty ellipse. (b) ML surface after three maneuvers.

4×4 approach the next array position is determined by using (18) with a circle constraint. A circle of radius 25 cm is used, and the array at position-2 is used as the reference with respect to which the next optimal array position is determined. The surface obtained by using the 4×4 FIM is shown in Fig. 13(a) and the values on the circle from -90° to 90° are shown in Fig. 13(b). Clearly there are two well defined peaks with one direction favored more than the other. The peak of this plot is picked to generate the next optimal array position. The next array positions are obtained optimally and the surface plot at step 4 and at the last step are shown in Fig. 14. There are couple of interesting observations, the optimal maneuvers pick one target and move toward it, and at the same time as the array moves toward target-1, the signature of target-2 becomes weak. At the last step the target-1 has been localized completely with appreciable reduction in the size of the uncertainty ellipse. However, the weak signature of target-2 is still somewhat present, and with a very accurate position estimate. Once we have completely localized one target, we would return to the original starting positions and remove the effects of the already localized target from the array data. The remaining targets can then be localized. The technique used will be the one based on the CLEAN algorithm originally developed for radio astronomy [9, 17]. Suppose that there are M targets, and out of these we have estimated all the positions except the m^{th} target. Then the new array data at a frequency ω_l which can be used for this target is given by:

$$\mathbf{y}_m(\omega_l) = \mathbf{y}(\omega_l) - \sum_{j=1, j \neq m}^M \mathbf{g}(\mathbf{p}_j, \omega_l) s_j(\omega_l) \quad (20)$$

where \mathbf{g} is the steering vector whose elements are given by a 2D Green's function, \mathbf{p}_j is the j^{th} target position

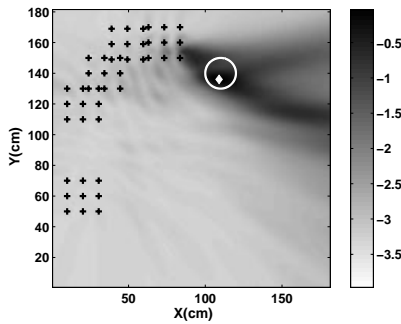


Figure 11. The final target position estimate is shown. The resolution of the image around the true target position is significantly increased after the optimal array movements (dB scale, inverse of the cost function is plotted).

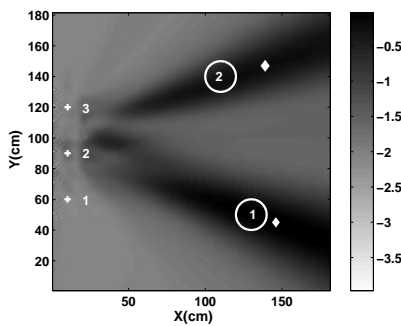


Figure 12. Probe Phase: Initial target location estimate is done using the ML cost function (10) (dB scale, inverse of the cost function is plotted). Three fixed array at positions 1, 2 and 3 are used. Only the center position of array is shown. The position of two targets (circles) and their initial estimates are also shown (diamonds).

estimate, and $s_j(\omega_l)$ is the signal reflected from the j^{th} target and its value is calculated using (9). Once we remove the first target using (20), the FIM will be reduced in size. The probe phase for the second target uses the previous starting position as shown in Fig. 15(a). The only difference is that the effect of target-1 has already been completely removed from the array data. The new array data is then used to determine the target position. The next few optimal moves to locate target-2 are shown in Fig. 15(b). Clearly this target has been completely localized in addition to considerable reduction in the size of its uncertainty ellipse.

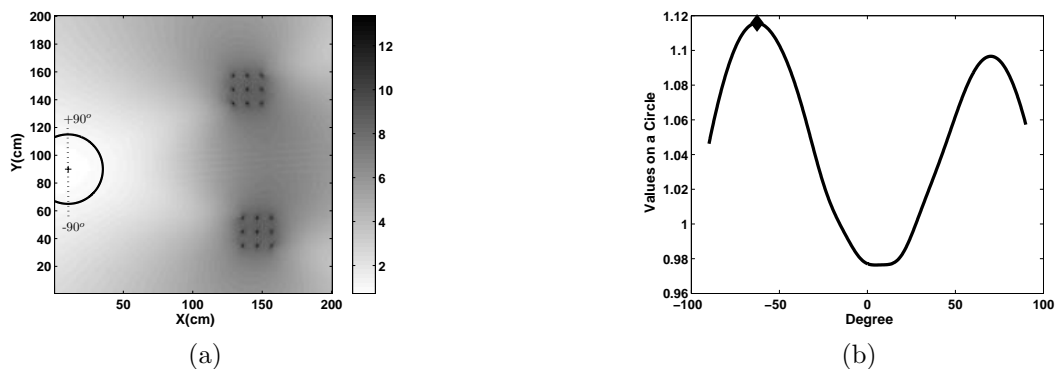


Figure 13. Next optimal array position (linear scale) (a) Surface plot obtained by (18) with a circle of 25 cm (b) Values obtained on the circle from -90° to 90° .

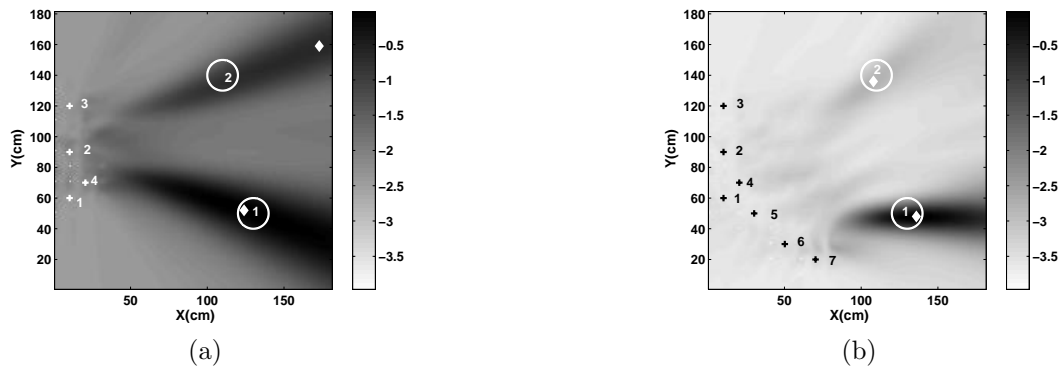


Figure 14. Other optimal maneuvers for the target position estimation are shown (dB scale, inverse of the cost function is plotted) (a) Step 4. (b) Step 7 (last step).

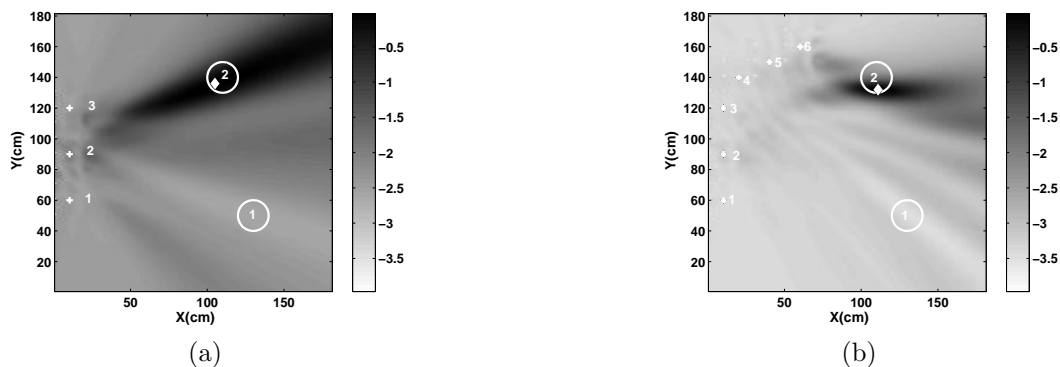


Figure 15. Target-2 position estimates after removing the effect of target-1 from the array (dB scale, inverse of the cost function is plotted) (a) Probe Phase which uses the array at position 1, 2 and 3. (b) Final estimate after three optimal maneuvers.

8. CONCLUSIONS

The algorithm presented in this paper shows that it is possible to control a maneuvering array to find buried targets. A complete mine finding system would require one more step to distinguish a land mine from clutter. Since the maneuver algorithm can obtain very accurate estimate of the target location, the array would be positioned to exploit the “resonance property” of buried land mines to make the confirmation. It is known that a seismic surface wave induces a considerable resonance in the buried land mines [3]. However, to isolate and identify the resonance, a different imaging algorithm [4] must be employed and the measurement has to be done on top of the mine.

Acknowledgment

This work is supported by the U.S. Army Research Office under contract number DAAD19-02-1-0252.

REFERENCES

1. W. R. Scott, Jr., G. D. Larson, J. S. Martin, and G. S. M. II, “Field testing and development of a seismic landmine detection system,” in *SPIE Proc.* **5089**, (Orlando, FL), April 2003.
2. W. R. Scott, Jr., J. S. Martin, and G. D. Larson, “Experimental model for a seismic landmine detection system,” *IEEE Trans. Geoscience and Remote Sensing* **39**, pp. 1155–1164, June 2001.
3. C. T. Schroder, *On the Interaction of Elastic Waves with Buried Landmines: An Investigation Using the Finite-Difference Time-Domain Method*. PhD thesis, Georgia Institute of Technology, Atlanta, GA, 2001.

4. A. Behoodian, W. R. Scott, Jr., and J. H. McClellan., "Signal processing of elastic surface waves for localizing landmines," in *33th Asilomar Conference on Signals, Systems, and Computers*, (Pacific Grove, CA), 1999.
5. V. V. Fedorov, ed., *Theory of Optimal Experiments*, SIAM, 1972.
6. X. Liao and L. Carin, "Application of the theory of optimal experiments to adaptive electromagnetic-induction sensing of buried targets," *IEEE Trans. on Pattern Analysis and Machine Intelligence* **26**, pp. 961–972, August 2004.
7. M. Alam and J. H. McClellan, "Near field imaging of subsurface targets using active arrays and elastic waves," in *11th IEEE DSP Workshop*, **5415**, (Taos Ski Valley, NM), August 2004.
8. M. Alam, J. H. McClellan, P. Norville, and W. R. Scott, Jr., "Time-reverse imaging for the detection of landmines," in *SPIE Proc*, **5415**, (Orlando, FL), April 2004.
9. M. Alam and J. H. McClellan, "Near field imaging of subsurface targets using wide-band multi-static RELAX/CLEAN algorithms," in *ICASSP 2005*, (Philadelphia), March 2004.
10. C. Prada and J. Thomas, "Experimental subwavelength localization of scatterers by decomposition of the time reversal operator interpreted as a covariance matrix," *J. Acoust. Soc. Am.* **114**, pp. 235–243, 2003.
11. D. Johnson and D. Dudgeon, *Array Signal Processing: Concepts and Techniques*, Prentice Hall, 1993.
12. L. Borcea, G. Papanicolaou, C. Tsokgka, and J. Berryman, "Imaging and time reversal in random media," *Inverse Problems* **18**, pp. 1247–1279, 2002.
13. M. Alam, J. H. McClellan, and W. R. Scott, Jr., "Multi-channel spectrum analysis of surface waves," in *37th Asilomar Conference on Signals, Systems, and Computers*, (Pacific Grove, CA), 2003.
14. V. Cevher, *A Bayesian Framework for target tracking using Acoustic and Image measurements*. PhD thesis, Georgia Institute of Technology, Atlanta, GA, 2005.
15. V. Cevher and J. H. McClellan, "Acoustic node calibration using a moving source." Accepted for publication in *IEEE Trans. on AES*.
16. Y. Zhou, P. Yip, and H. Leung, "Tracking the direction-of-arrival of multiple moving targets by passive arrays: Algorithm," *IEEE Trans. on Signal Processing* **47**(10), pp. 2655–2666, October 1999.
17. Y. Wang, J. Li, P. Stoica, M. Shepalk, and T. Nishida, "Wideband relax and wideband clean for aeroacoustic imaging," *J. Acoust. Soc. Am.(JASA)* **115**(2), pp. 757–767, 2004.